

Numerical Investigation of the Effect of Wire Screen Mesh Specification and Evaporator Length on Thermal Performance of Cylindrical Heat Pipe

Hassanain Ghani Hameed
Foundation of Technical Education
Engineering Technical College/ Najaf
Automobile Department

Proof. Dr. Abudl-Muhsin A. Rageb
University of Basra
Engineering College
Mechanical Engineering Department

Abstract

A numerical model has been developed to determine the effect of the wire screen mesh (wick) type on the heat transfer performance of copper–water wicked heat pipe. This model represented as steady-state incompressible flow. The governing equations in cylindrical coordinates have been solved in vapor region, wick structure and wall region, using finite difference with forward-backward upwind scheme. The results show that increasing the mesh number led to decreasing the maximum heat transfer limit and increasing the capillary pressure. While, for the same heat input the operating temperature of the heat pipe increase when the mesh number increase. Also, it was found that increasing the evaporation length, with constant condensation length, decrease the operating temperature and increase the maximum heat transfer limit. For verification of the current model, the results of liquid pressure drop for a heat pipe have been compared with the previous study for the same problem and a good agreement has been achieved.

أ.د. عبد المحسن عبود رجب
جامعة البصرة
كلية الهندسة
قسم الهندسة الميكانيكية

حسين غني حميد
هيئة التعليم التقني
الكلية التقنية الهندسية / النجف
قسم هندسة تقنيات السيارات

الخلاصة

تم تطوير نموذج عددي لحساب تأثير نوع الفتيل الشبكي على اداء انتقال الحرارة لأنبوب حراري ذو فتيل شبكي من الداخل ومصنوع من النحاس ويستخدم الماء كمائع للعمل. هذا النموذج مثل كجريان لا انضغاطي في الحالة المستقرة. المعادلات الحاكمة بصيغة الاحداثيات الاسطوانية حلت في مناطق البخار، الفتيل الشبكي وجدار الانبوب، باستخدام طريقة الفروقات المحددة مع نظام امام-خلف مع الريح. النتائج بينت ان زيادة رقم الشبكة يؤدي الى نقصان حد انتقال الحرارة الاعظم وزيادة الضغط الشعيري. بينما، لنفس كمية الحرارة الداخلة فان درجة حرارة العمل للأنبوب الحراري تزداد مع زيادة رقم الشبكة. ايضا، وجد بان زيادة طول المبخر، مع بقاء طول المكثف ثابت، يقلل درجة حرارة العمل ويزيد حد انتقال الحرارة الاعظم. من اجل التأكد من صحة النموذج الحالي، فان نتائج هبوط ضغط الماء للأنبوب الحراري قورنت مع الدراسة السابقة لنفس المسألة وكان هنالك توافق جيد.

Keywords: Cylindrical heat pipe; Wire screen mesh; Numerical model.

Nomenclature

A = area (m^2)

C_p = heat capacity at constant pressure (kJ/kg. K)

h = convective heat transfer coefficient ($W/m^2 \cdot K$)

h_{fg} = latent heat of vaporization (kJ/kg)

k = thermal conductivity (W/m. K)

k_{eff} = effective thermal conductivity of the

liquid-saturated wick (W/m. K)

K_p = permeability of the wick (m^2)

L = length (m)

L_{eff} = effective length of heat pipe (m)

P = pressure (N/m^2)

Q = heat transfer (W)

r = radial coordinate (m)

r_c = capillary radius of wick (m)

R = gas constant (kJ/kg. K)

R_{th} = thermal resistance (K/W)
 Re = Reynolds number
 Pr = Prandtl number
 T = temperature (K)
 u = axial velocity (m/s)
 v = radial vapor velocity (m/s)
 V = reference velocity (m/s)
 x = axial coordinate (m)

Greek Symbols

ε = porosity of the wick
 σ = surface tension of the working liquid (N/m)
 Ψ = stream function (m³/s)
 ω = vorticity (sec⁻¹)
 α = fluid thermal diffusivity (m²/sec)
 ν = kinematics viscosity (m²/sec)
 μ = dynamic viscosity (kg/m. sec)
 ρ = density (kg/m³)
 β = inclination angle of heat pipe (degree)
 θ = dimensionless temperature

Subscripts

* = dimensionless term
 a = adiabatic
 c = condenser
 col = coolant
 e = evaporator
 in = inlet
 int = interface
 l = liquid
 o = outer
 s = sink, solid
 sat = saturated
 set = set point
 sur = surrounding
 v = vapor
 w = wick
 wa = wall

Superscripts

$\bar{\quad}$ = average quantity

1. Introduction

The early work on the heat pipes was presented in the mid of the last century. Heat pipes are widely used in many different engineering applications. The most important advantage of using heat pipes is the efficient and rapid for heat transporting that is much better than using pure metal only such as

copper.

The effective thermal resistance and maximum heat transfer limit are the main parameters that characterize the thermal performance of the heat pipes [1,2]. In many moderate-temperature applications, the heat transport rate is mainly related to the capillary pressure that is generated by the wick structure [2]. Therefore, most of the researches that study the heat pipe focused on developing better models to predict the pressure drop that occurs in wicked heat pipes. Investigations in this field included numerical and analytical methods that have solved the coupled equations for liquid flow through the wick and the vapor flow for range of different conditions, including multiple heat sources and transient start-up of the heat pipe [3–8].

In general, for the prediction of the thermal performance of the heat pipe, a one-dimensional thermal resistance network is used, where each component of the heat pipe is modeled by an associated thermal resistance.

It has been proven that in typical low-temperature applications, the thermal resistance of the saturated wick structure in the evaporator and condenser regions accounts for much of the thermal resistance of the heat pipe [9]. Thus, accurate models for the heat transfer through these sections of wick are important for predicting the effective thermal resistance of a wicked heat pipe. Through the saturated wick, the evaporation or condensation at the surface, in most cases, occurs due to the heat transfer at the evaporator and condenser sections by conduction which represents the upper limit of the thermal resistance of the wick.

Many researches focused on the study of the effective thermal conductivity of saturated screen mesh wicks by developing a number of empirical, semi-empirical and analytical models. The predictions from these models differ by an order of magnitude for the same wick structure. The thermal resistance of the saturated wick is relatively independent of heat flux, however, it mainly depends on the geometry and properties of the wick and the conductivity of the working fluid [9]. The non-linearity in the overall thermal resistance of screen mesh wicked heat pipes has been proven

by several experiments, particularly at low heat fluxes [9,10].

In this paper a numerical model to study the effect of wick specification and evaporator length on the operation of heat pipe is presented. A finite difference method to solve the steady state incompressible flow in cylindrical coordinates in vapor region, wick structure and wall region is used. The Darcy's law is implemented for momentum equation in porous media. The objective of this paper is to study the wick specification variation on the operation of a conventional heat pipe.

2. Mathematical Model

A cylindrical heat pipe as shown in Fig. 1 consists of three parts:

1. Evaporator section,

2. Adiabatic (transport) section

3. Condenser section.

Basically, the heat is transferred from source to a heat sink based on evaporating-condensing loop inside the heat pipe. Where it is sealed and vacuum-pumped vessels that partially filled with liquid. The internal walls are lined with a porous medium, named the wick, that acts as a passive capillary pump. When the heat is applied at one end, the liquid begins to vaporize which results in a pressure gradient that causes the vapor to flow towards the cooler region. At the cooler end the vapor condenses and transported back by the wick structure and hence, the process is repeated as long as there is sufficient capillary pressure to drive the condensate back to the evaporator through the wick.

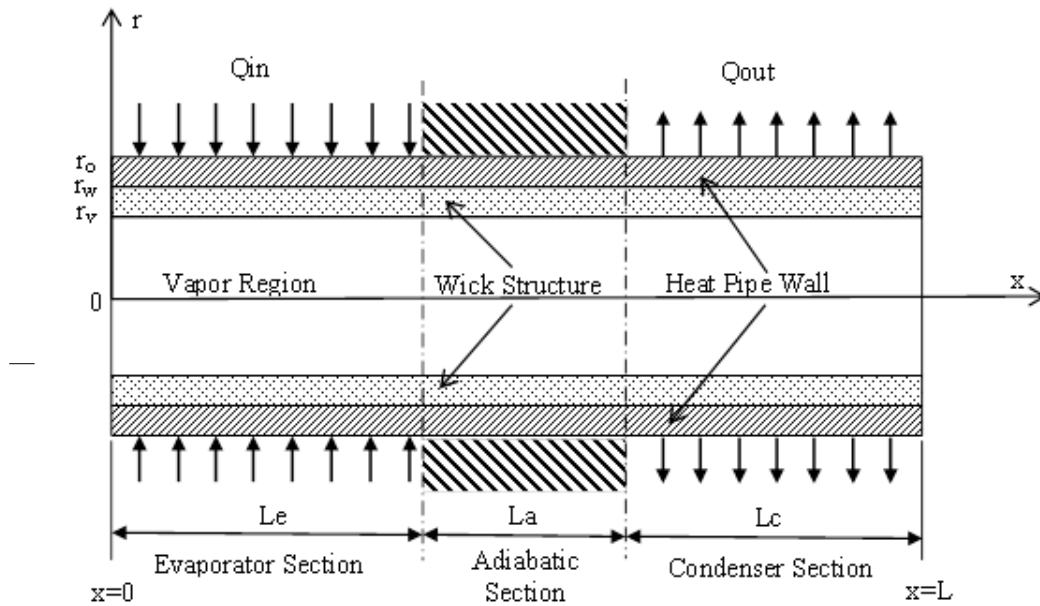


Fig. 1. Schematic of a cylindrical heat pipe under consideration.

2.1 Governing Equations and Boundary Conditions

The model for steady state two dimensional incompressible laminar flow has been solved in cylindrical coordinates in vapor region, wick structure and wall region. The wick is assumed isotropic and saturated with the working liquid. The vapor injection and suction at the liquid-vapor interface are assumed to be uniform.

i- Vapor Region

The governing equations in vapor region are continuity, Navier-Stokes and energy equations as follows, [11]:

$$\frac{\partial u}{\partial x} + \frac{1}{r} \frac{\partial(rv)}{\partial r} = 0 \quad (1)$$

$$\rho u \frac{\partial u}{\partial x} + \rho v \frac{\partial u}{\partial r} = -\frac{\partial p}{\partial x} + \mu \left[\frac{\partial^2 u}{\partial x^2} + \frac{1}{r} \frac{\partial u}{\partial r} + \frac{\partial^2 u}{\partial r^2} \right] \quad (2)$$

$$\rho u \frac{\partial v}{\partial x} + \rho v \frac{\partial v}{\partial r} = -\frac{\partial p}{\partial r} + \mu \left[\frac{\partial^2 v}{\partial x^2} + \frac{1}{r} \frac{\partial v}{\partial r} + \frac{\partial^2 v}{\partial r^2} - \frac{v}{r^2} \right] \quad (3)$$

$$\rho C_p \left[u \frac{\partial T}{\partial x} + v \frac{\partial T}{\partial r} \right] = k \left[\frac{\partial^2 T}{\partial x^2} + \frac{1}{r} \frac{\partial T}{\partial r} + \frac{\partial^2 T}{\partial r^2} \right] \quad (4)$$

The boundary conditions for vapor region are as following:

The radial velocities at liquid-vapor interface [12]:

$$\begin{cases} v_e = + \frac{Q_e}{2\pi r_v L_e \rho_v h_{fg}} & 0 \leq x \leq L_e \\ v_a = 0 & L_e \leq x \leq L_e + L_a \\ v_c = - \frac{Q_c}{2\pi r_v L_c \rho_v h_{fg}} & L_e + L_a \leq x \leq L_e + L_a + L_c \end{cases} \quad (5)$$

The temperature at the vapor-liquid interface of the evaporator and condenser is calculated approximately using Clausius-Clapeyron equation,[12].

$$T_{\text{int}} = \frac{1}{\frac{1}{T_{v,\text{sat}}} - \frac{R}{h_{fg}} \ln \frac{P_v}{P_{v,\text{sat}}}} \quad (6)$$

The boundary conditions at both pipe ends are:

$$v = u = 0 \quad \frac{\partial T}{\partial x} = 0 \quad (7)$$

At pipe centerline the symmetry boundary conditions are:

$$v = 0, \quad \frac{\partial u}{\partial r} = 0 \quad \& \quad \frac{\partial T}{\partial r} = 0 \quad (8)$$

ii- Wick Structure

The governing equations in wick structure are as follows, [13,14]:

$$\frac{\partial u}{\partial x} + \frac{1}{r} \frac{\partial(rv)}{\partial r} = 0 \quad (9)$$

The Darcy's law has been employed for momentum equation in porous media:

$$\rho u \frac{\partial u}{\partial x} + \rho v \frac{\partial u}{\partial r} = - \frac{\partial p}{\partial x} + \mu \left[\frac{\partial^2 u}{\partial x^2} + \frac{1}{r} \frac{\partial u}{\partial r} + \frac{\partial^2 u}{\partial r^2} \right] - \frac{\varepsilon \mu}{K_p} u - \frac{\varepsilon^2 F}{K_p^{1/2}} \rho |u| u \quad (10)$$

$$\rho u \frac{\partial v}{\partial x} + \rho v \frac{\partial v}{\partial r} = - \frac{\partial p}{\partial r} + \mu \left[\frac{\partial^2 v}{\partial x^2} + \frac{1}{r} \frac{\partial v}{\partial r} + \frac{\partial^2 v}{\partial r^2} - \frac{v}{r^2} \right] - \frac{\varepsilon \mu}{K_p} v - \frac{\varepsilon^2 F}{K_p^{1/2}} \rho |v| v \quad (11)$$

$$(\rho C_p)_{\text{eff}} \left[u \frac{\partial T}{\partial x} + v \frac{\partial T}{\partial r} \right] = k_{\text{eff}} \left[\frac{\partial^2 T}{\partial x^2} + \frac{1}{r} \frac{\partial T}{\partial r} + \frac{\partial^2 T}{\partial r^2} \right] + S \quad (12)$$

F is a geometric function based on the porous wick structure and is calculated as follows,[3]:

$$F = 1.75 / \sqrt{150} \varepsilon^{3/2} \quad (13)$$

The effective thermal conductivity and heat capacity of wick structure, are calculated from equations for screen wire mesh, [13,15]

$$k_{\text{eff}} = \frac{k_l [(k_l + k_s) - (1 - \varepsilon)(k_l + k_s)]}{[(k_l + k_s) + (1 - \varepsilon)(k_l - k_s)]} \quad (14)$$

$$(\rho C_p)_{\text{eff}} = \varepsilon (\rho C_p)_l + (1 - \varepsilon) (\rho C_p)_s \quad (15)$$

Since the phase change phenomena was not included in current model, for modeling latent heat of vaporization a heat sink was employed in evaporator section and a heat source was used in condenser section. The values of these terms are[14]:

$$\begin{cases} S_e = - \frac{Q_e}{\pi(r_w^2 - r_v^2)L_e} \\ S_a = 0 \\ S_c = + \frac{Q_c}{\pi(r_w^2 - r_v^2)L_c} \end{cases} \quad (16)$$

The boundary conditions for wick structure are as following:

The radial velocities at liquid-vapor interface [13]:

$$\begin{cases} v_e = - \frac{Q_e}{2\pi r_v L_e \rho_v h_{fg} \varepsilon} & 0 \leq x \leq L_e \\ v_a = 0 & L_e \leq x \leq L_e + L_a \\ v_c = + \frac{Q_c}{2\pi r_v L_c \rho_v h_{fg} \varepsilon} & L_e + L_a \leq x \leq L_e + L_a + L_c \end{cases} \quad (17)$$

The temperature at the liquid - vapor interface of the evaporator and condenser is calculated approximately using Clausius-Clapeyron equation, as shown previously in equation (6).

The boundary conditions at both pipe ends are:

$$v = u = 0 \quad \frac{\partial T}{\partial x} = 0 \quad (18)$$

At wick-wall interface:

$$\begin{cases} k_{eff} \frac{\partial T_w}{\partial r} = k_{wa} \frac{\partial T_{wa}}{\partial r} \\ T_w = T_{wa} \end{cases} \quad (19)$$

iii- Wall Region

At heat pipe wall the equation of thermal conduction was used in cylindrical coordinates, [14]:

$$\left[\frac{\partial^2 T_{wa}}{\partial x^2} + \frac{1}{r} \frac{\partial T_{wa}}{\partial r} + \frac{\partial^2 T_{wa}}{\partial r^2} \right] = 0 \quad (20)$$

The boundary conditions in this region are as following:

At both ends of heat pipe:

$$\frac{\partial T_{wa}}{\partial x} = 0 \quad (21)$$

At wall-wick interface, the boundary condition as in equation (19):

At heat pipe external surface:

$$\begin{cases} k_{wa} \frac{\partial T_{wa}}{\partial r} = + \frac{Q_e}{2\pi r_o L_e} & 0 \leq x \leq L_e \\ \frac{\partial T_{wa}}{\partial r} = 0 & L_e \leq x \leq L_e + L_a \\ k_{wa} \frac{\partial T_{wa}}{\partial r} = -h(T_o - T_s) & L_e + L_a \leq x \leq L_e + L_a + L_c \end{cases} \quad (22)$$

In conventional heat pipes, under steady-state operation, there exists a maximum capillary pressure that can be developed in wick structure. The maximum heat transport capillary limit for a heat pipe is achieved when the sum of the pressure losses along the circulation path of the working fluid reaches the maximum capillary pressure; that is

$$\Delta p_{cap} = \Delta p_v + \Delta p_l + \Delta p_g = \frac{2 \cos \theta \sigma_l}{r_c} \quad (23)$$

Δp_v can be neglecting, and substituting for pressure terms in equation (23), [16]. Gives:

$$\frac{2 \cos \theta \sigma_l}{r_c} = \left(\frac{\mu_l}{\rho_l} \right) \left(\frac{L_{eff} \dot{m}_{max}}{A_w K_p} \right) + \rho_l g L_{eff} \sin \beta \quad (24)$$

$$L_{eff} = \frac{1}{2} (L_e + 2L_a + L_c) \quad (25)$$

For water as working fluid and horizontal heat pipe the maximum liquid flow rate in the wick become:

$$\dot{m}_{max} = \left(\frac{\rho_l A_w K_p}{\mu_l L_{eff}} \right) \left(\frac{2 \sigma_l}{r_c} \right) \quad (26)$$

Thus, the maximum heat transport capillary limit may be written as, [16]:

$$Q_{max} = \dot{m}_{max} h_{fg} \quad (27)$$

$$Q_{max} = \left(\frac{\rho_l A_w K_p h_{fg}}{\mu_l L_{eff}} \right) \left(\frac{2 \sigma_l}{r_c} \right)$$

The saturation temperature inside the heat pipe can be calculated from the following equation, [17]:

$$T_{sat} = \left(\frac{Q_c}{Q_{max}} \right) (T_{set} - T_s) + T_s \quad (28)$$

The thermal resistance, which represent the effectiveness of the heat pipe can be calculated from the following equation:

$$R_{th} = \frac{\bar{T}_e - \bar{T}_c}{Q_{in}} \quad (29)$$

3. Method Of Solution

The governing equations are discretized using a finite difference approach and the equations are solved using Forward – Backward upwind with collocated grid scheme. Various numbers of meshes are used as shown in figure 2, and 9881 nodes were sufficient to achieve results that were independent to mesh structure. The computation is done for a mesh number (241×41) in axial and radial direction respectively. The physical domain of problem was classified into three regions as follows:

1. vapour region
2. wick structure
3. wall region

It is convenient, for the numerical

analysis, to use the governing equations in terms of stream function and vorticity as:

$$u = \frac{1}{r} \frac{\partial \psi}{\partial r} \quad (30)$$

$$v = -\frac{1}{r} \frac{\partial \psi}{\partial x} \quad (31)$$

$$\omega = \frac{\partial v}{\partial x} - \frac{\partial u}{\partial r} \quad (32)$$

Using the above equations, and eliminating the pressure term, the governing equations are transformed to:

$$\omega = -\frac{1}{r} \frac{\partial^2 \psi}{\partial x^2} - \frac{1}{r} \frac{\partial^2 \psi}{\partial r^2} + \frac{1}{r^2} \frac{\partial \psi}{\partial r} \quad (33)$$

$$\frac{1}{r} \left[\frac{\partial \psi}{\partial r} \frac{\partial \omega}{\partial x} - \frac{\partial \psi}{\partial x} \frac{\partial \omega}{\partial r} \right] + \frac{\omega}{r^2} \frac{\partial \psi}{\partial x} = \quad (34)$$

$$v \left[\frac{\partial^2 \omega}{\partial x^2} + \frac{\partial^2 \omega}{\partial r^2} + \frac{1}{r} \frac{\partial \omega}{\partial r} - \frac{1}{r^2} \omega \right] \quad (35)$$

$$\frac{1}{r} \left[\frac{\partial \psi}{\partial r} \frac{\partial T}{\partial x} - \frac{\partial \psi}{\partial x} \frac{\partial T}{\partial r} \right] = \alpha \left[\frac{\partial^2 T}{\partial x^2} + \frac{1}{r} \frac{\partial T}{\partial r} + \frac{\partial^2 T}{\partial r^2} \right]$$

Now, after obtained the governing equations in terms of stream function and vorticity, then they with the corresponding boundary conditions are transferred to the non-dimensional form using the following dimensionless quantities:

$$x^* = \frac{x}{r_o}; r^* = \frac{r}{r_o}; u^* = \frac{u}{V}; v^* = \frac{v}{V}; \psi^* = \frac{\psi}{V r_o^2}; \omega^* = \frac{\omega r_o}{V} \quad (36)$$

$$p^* = \frac{p}{\frac{1}{2} \rho V^2}; \theta = \frac{T - T_s}{T_{sat} - T_s}; Pr = \frac{\mu C_p}{k}; Re = \frac{V r_o}{\nu}$$

The solution procedure of the discretized equations is based on a line-by-line iteration method in the axial and radial directions using Fortran Power Station program. The solution procedure of the numerical analysis which performed in the above separated region is as follows:

1. Continuity and momentum equation are solved in vapor region with mentioned boundary conditions to find the pressure

distribution after obtaining the velocity components (u and v).

2. Equation (6) has been used in dimensionless form to find temperature boundary condition at the vapor-liquid interface.

3. The energy equation is solved in vapor region.

4. The mentioned equations with related boundary conditions have been solved in the wick structure and pipe wall region.

The above procedure repeated until the convergence is achieved with relative error for the calculated parameters (ψ , ω , p and θ) equal to $5 * 10^{-5}$.

4. Results And Discussion

A cylindrical horizontal heat pipe with distilled water as working fluid is selected. The specifications of the heat pipe and the wicks are shown in table 1 and 2.

Figures 3 – 11 show the dimensionless contours plot for liquid pressure, temperature distribution and stream line inside the heat pipe for different values of heat transfer rate and different wick type, while the evaporator length equal to 1.546 of the condenser length.

For the same wick, when the heat transfer rate increase the mass flow rate increased so that the radial and axial velocities increased, which lead to increase the liquid pressure, temperature and stream line values. Also, due to increasing the heat transfer rate the saturation pressure will increase, which in turn lead to increase the heat pipe operation temperature. While, for different wick type, the saturation pressure and in turn the saturation temperature are increased when the mesh number increased due to decreasing the wick permeability, which led to decreasing the capillary heat transfer limit and thus the dimensionless parameters (ψ , and p) are increased as a result of the saturation temperature increasing.

Figures 12 and 13 show the dimensionless contours plot for liquid pressure, temperature distribution and stream line inside the heat pipe for heat transfer rate of 15 W and wick type-2 with evaporator length equal to 2.99 and 4.721 of the condenser length respectively. It is shown from the figures, when

the evaporator length increased the liquid pressure, temperature distribution and stream line are decreased due to reducing the adiabatic length which in turn led to decreasing the effective operation length (L_{eff}).

Figure 14 illustrates the effect of wick type on the capillary heat transfer limit and the capillary pressure at heat input of 25 Watt. Whereas, increasing the mesh number lead to decreasing the capillary heat transfer limit and increasing the capillary pressure, due to decreasing the wick thickness and decreasing the capillary radius of the wick.

The effect of wick type on the thermal resistance for different heat input is shown in figure 14. The thermal resistance decreases with the mesh number and then approaches a constant value. This due to decreasing the evaporator-condenser temperature difference with increase the mesh number until reaches a constant difference value although the mesh number was increased.

The effect of evaporator length variation, when the condenser length was kept constant at heat input of 15 W, on the maximum

heat transfer limit, the operating temperature and the thermal resistance are shown in figure 16 and 17 respectively. Whereas, increasing the evaporator length led to increasing the maximum heat transfer limit, due to decreasing the effective working length (L_{eff}), which in turn led to decreasing the operating temperature. Also, increasing the evaporator length led to small increasing in the thermal resistance and then reaches a constant value although the evaporator length was increased, this due to the increase in the evaporator-condenser temperature difference and then reaches a constant value. It is show that increasing the evaporator length is desired to increase the heat pipe performance.

To verify the current numerical model of the heat pipe. the result of liquid pressure distribution along the heat pipe is compared with the result of (Mahjoub and Mahtabroshan, 2008) for the similar problem. Figure 18 show a good agreement for the liquid pressure distribution at 10 watt as transmitting heat power.

Table 1: Heat pipe specification.

Heat pipe wall material	Copper
Wall thickness	0.85mm
Outer diameter (t_{wall})	19.05mm
Heat pipe length (L)	555mm
Evaporator length (L_e)	1.546 L_c , 2.99 L_c , 4.721 L_c
Condenser length (L_c)	97mm
Working fluid	Distilled water
Sink temperature	18.3 °C
Set temperature	100 °C

Table 2: Wire screen mesh (wick) specification.

Wick type	mesh/in	mesh/m	wire diameter (mm)	calculated porosity	calculated permeability (m^2)
Wick (1)	100mesh	3937	0.08	0.7402	3.15E-10
Wick (2)	145mesh	5069	0.057	0.731	1.447E-10
Wick (3)	200mesh	7874	0.053	0.6557	5.476E-11

5. Conclusion

A numerical model is simulated for the

steady state two-dimensional heat transfer and flow equations in vapor region, porous media

and wall region. The governing equations have been solved using upwind finite difference with collocated grid scheme. Using this model, it is possible to study the effects of the wick specification and evaporator length on system behavior. The results show that, the working heat pipe temperature increase with increasing the mesh number. The thermal resistance and maximum heat transfer limit decreases with increasing of mesh number. Also, increasing the evaporator length enhance the heat pipe performance. This model has been verified with available numerical data and has shown good agreement.

References

- [1]-G.P. Peterson, *An Introduction to Heat Pipes: Modeling, Testing, and Applications*, John Wiley & Sons, New York, 1994.
- [2]-A. Faghri, *Heat Pipe Science and Technology*, Taylor & Francis, Washington, DC, 1995.
- [3]-N. Zhu, K. Vafai, Analysis of cylindrical heat pipes incorporating the effects of liquid–vapor coupling and non-Darcian transport – A closed form solution, *International Journal of Heat and Mass Transfer* 42 (1999) 3405–3418.
- [4]-J.M. Tournier, M.S. El-Genk, Startup of a horizontal lithium–molybdenum heat pipe from a frozen state, *International Journal of Heat and Mass Transfer* 46 (2003) 671–685.
- [5]-K.A.R. Ismail, M.A. Zanardi, A steady-state model for heat pipes of circular or rectangular cross-sections, *Journal of Applied Thermal Engineering* 16 (1996) 753–767.
- [6]-K.A.R. Ismail, R.F. Miranda, Two-dimensional axisymmetrical model for a rotating porous wicked heat pipe, *Journal of Applied Thermal Engineering* 17 (1997) 135–155.
- [7]-K.A.R. Ismail, M.M. Abogderah, Performance of a heat pipe solar collector, *Journal of Solar Engineering* 120 (1998) 51–59.
- [8]-H. Shabgard and A. Faghri, Performance characteristics of cylindrical heat pipes with multiple heat sources, *Journal of Applied Thermal Engineering* 31 (2011) 3410–3419.
- [9]-R. Kempers et al., Effect of number of mesh layers and fluid loading on the performance of screen mesh wicked heat pipes, *Journal of Applied Thermal Engineering* 26 (2006) 589–595.
- [10]- Y.M. Chen, S.C. Wu, C.I. Chu, Thermal performance of sintered miniature heat pipes, *Heat and Mass Transfer* 37 (2001) 611–616.
- [11]- Latif M. Jiji, *Heat Convection*, © Springer 2006.
- [12]- A. Nouri-Borujerdi, M. Layeghi, A Numerical Analysis of Vapor Flow in Concentric Annular Heat Pipes, *Transaction of ASME: Journal of Fluids Engineering*, Vol. 126, pp.442- 448, 2004.
- [13]- O. T. Fadhil, Numerical and Experimental Study on a Heat Pipe With Porous Media Wick, Ph.D. Thesis, university of Technology, 2006.
- [14]- S. Mahjoub, A. Mahtabroshan, Numerical Simulation of a Conventional Heat Pipe, *World Academy of Science, Engineering and Technology*, Vol. 39, pp. 117-122, 2008
- [15]- B. Rashidian, M. Amidpour and M. R. Jafari Nasr, Modeling the Transient Response of the Thermosyphon Heat Pipes, *Proceedings of the World Congress on Engineering*, Vol. II, London, U.K., 2008.
- [16]- D. Reay and P. Kew, *Heat Pipes: Theory, Design and Applications*, Fifth Edition, Elsevier, 2006.
- [17]- M. Cleary, R. Grimes, M. Hodes and M. T. North, Design of a Variable Conductance Heat Pipe for a Photonic Component, *Proceedings of IMECE2006* , Chicago, USA, 2006.

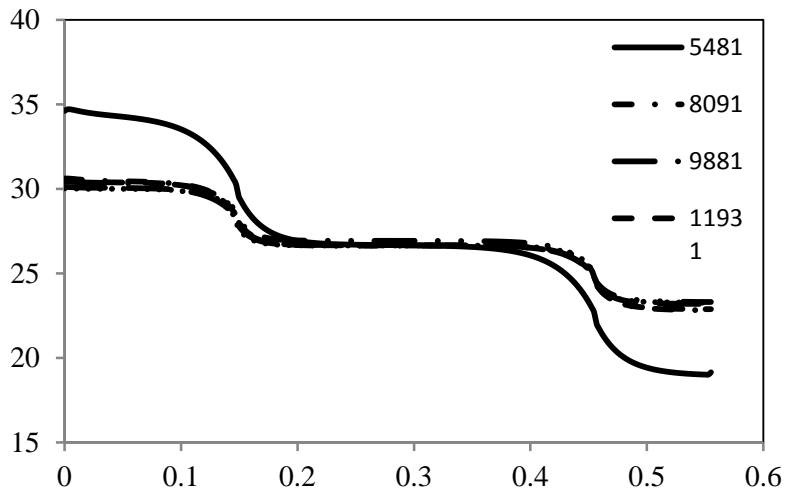


Figure 2: Checking for grid independency.

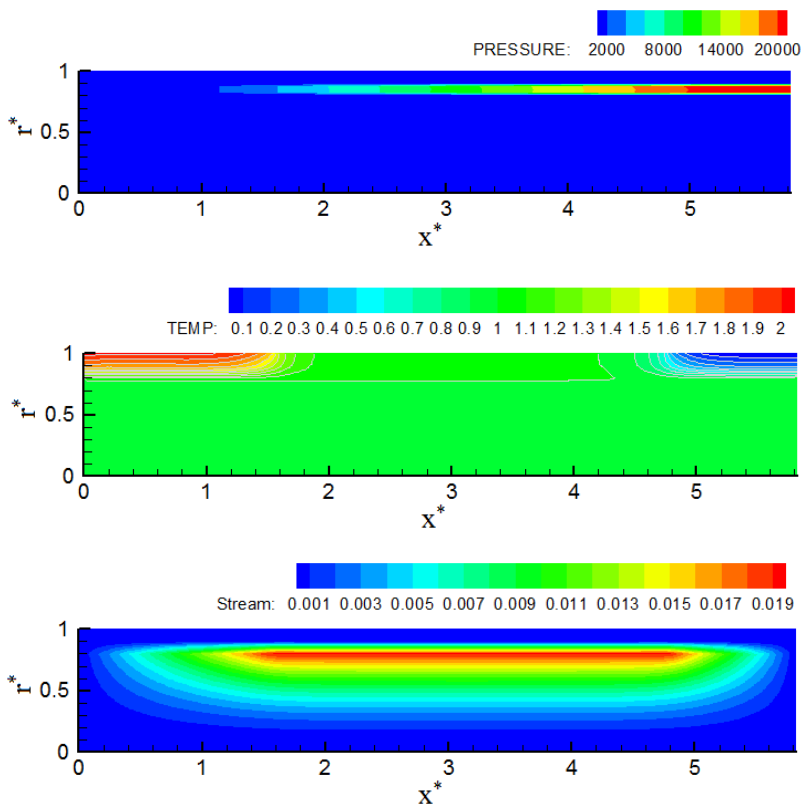


Figure 3: Dimensionless liquid pressure, temperature and Stream line distribution inside the heat pipe at $Q_{in}=5$ W and mesh number 100.

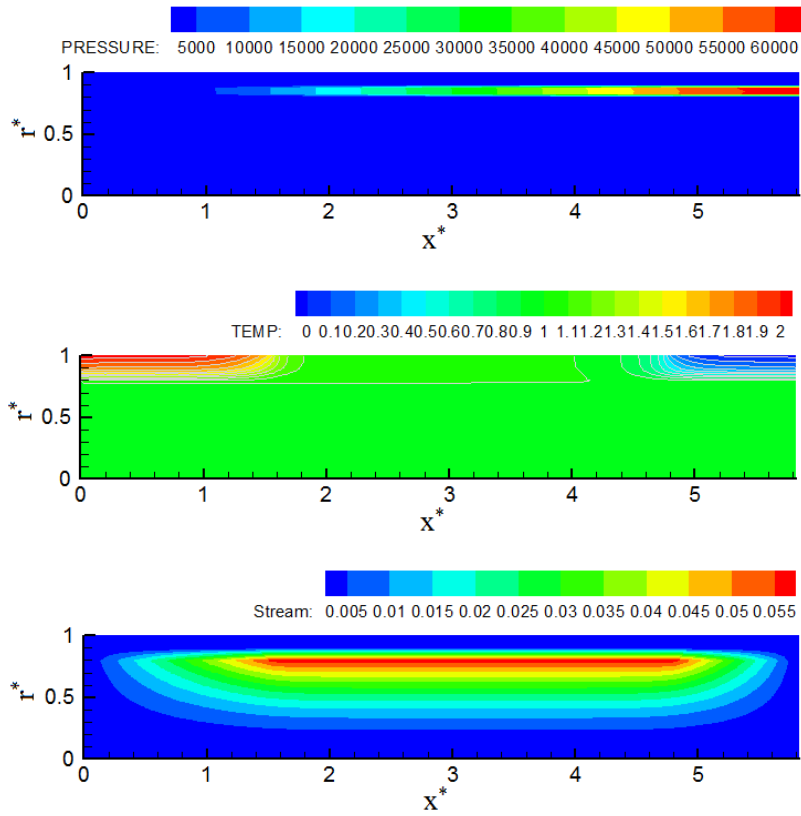


Figure 4: Dimensionless liquid pressure, temperature and Stream line distribution inside the heat pipe at $Q_{in}=15$ W and mesh number 100.

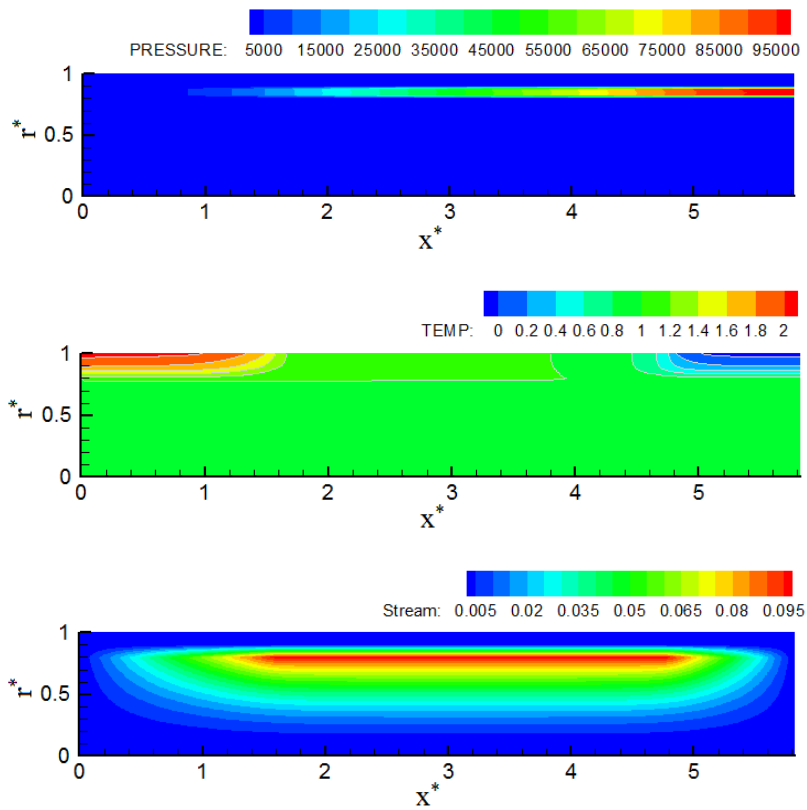


Figure 5: Dimensionless liquid pressure, temperature and Stream line distribution inside the heat pipe at $Q_{in}=25$ W and mesh number 100.

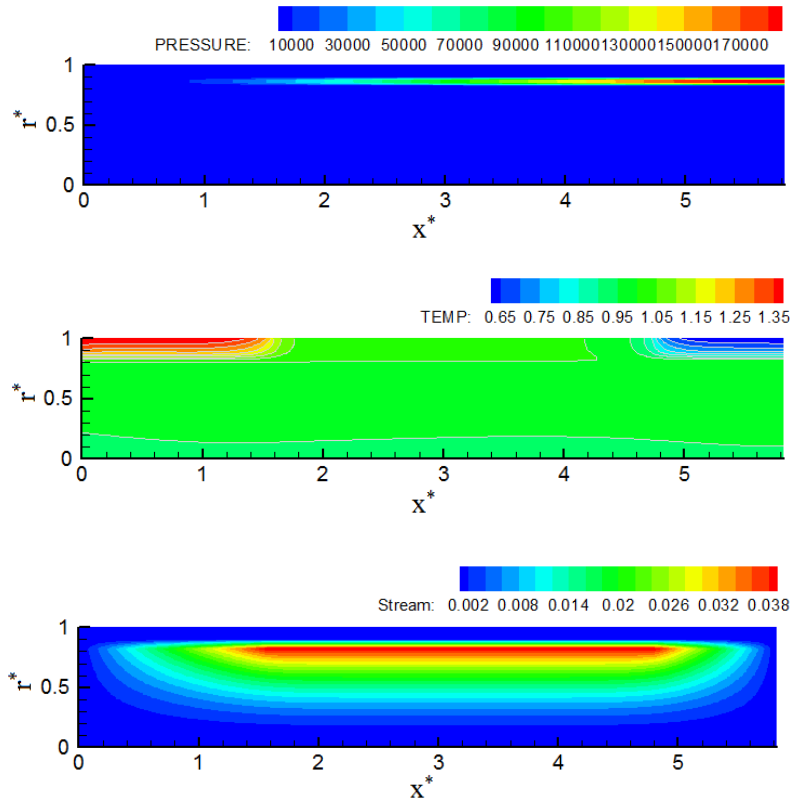


Figure 6: Dimensionless liquid pressure, temperature and Stream line distribution inside the heat pipe at $Q_{in}=5$ W and mesh number 145.

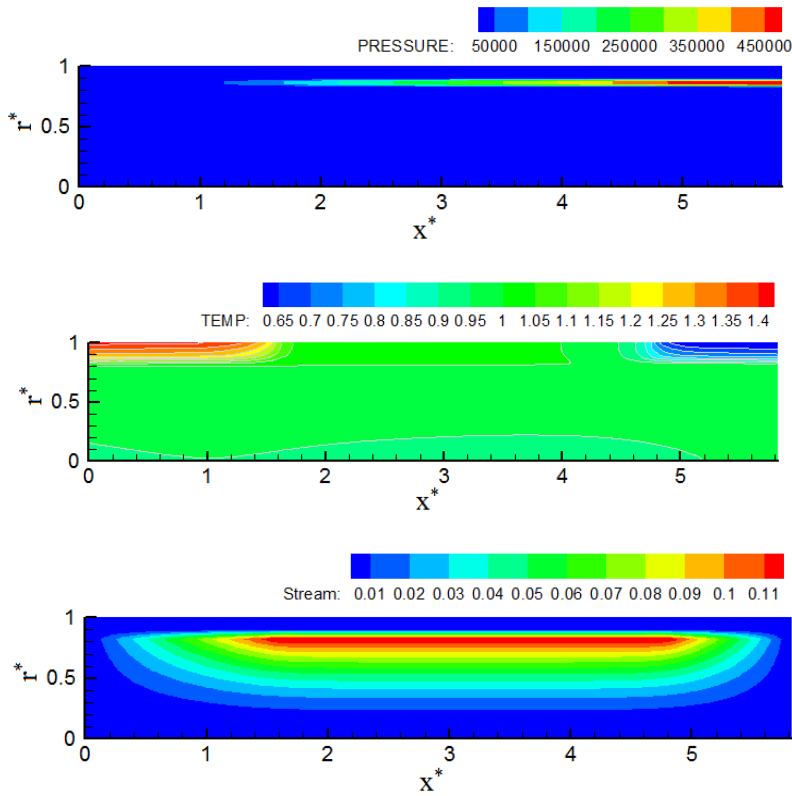


Figure 7: Dimensionless liquid pressure, temperature and Stream line distribution inside the heat pipe at $Q_{in}=15$ W and mesh number 145.

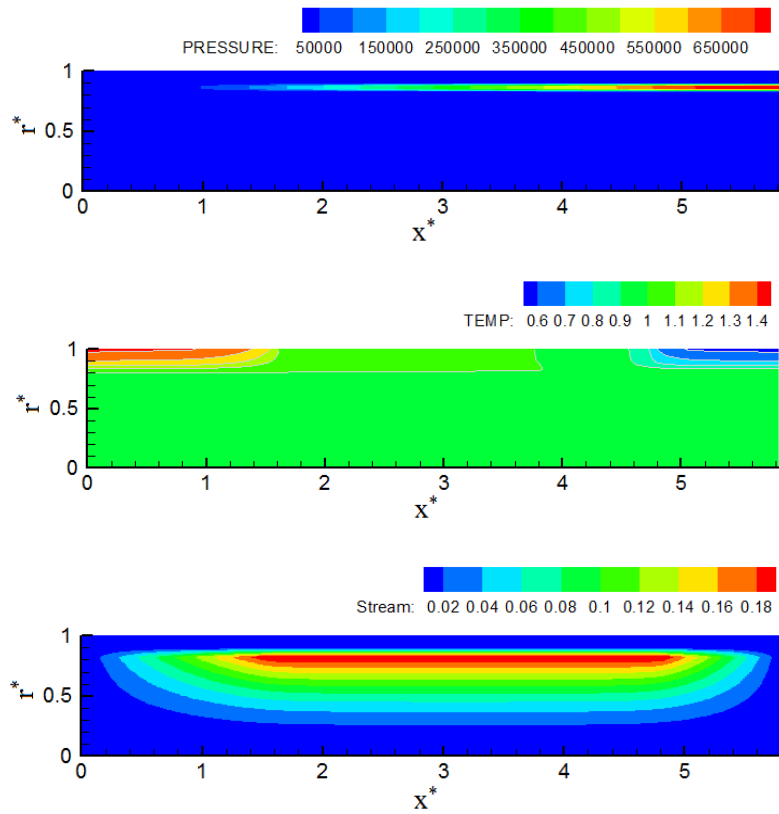


Figure 8: Dimensionless liquid pressure, temperature and Stream line distribution inside the heat pipe at $Q_{in}=25$ W and mesh number 145.

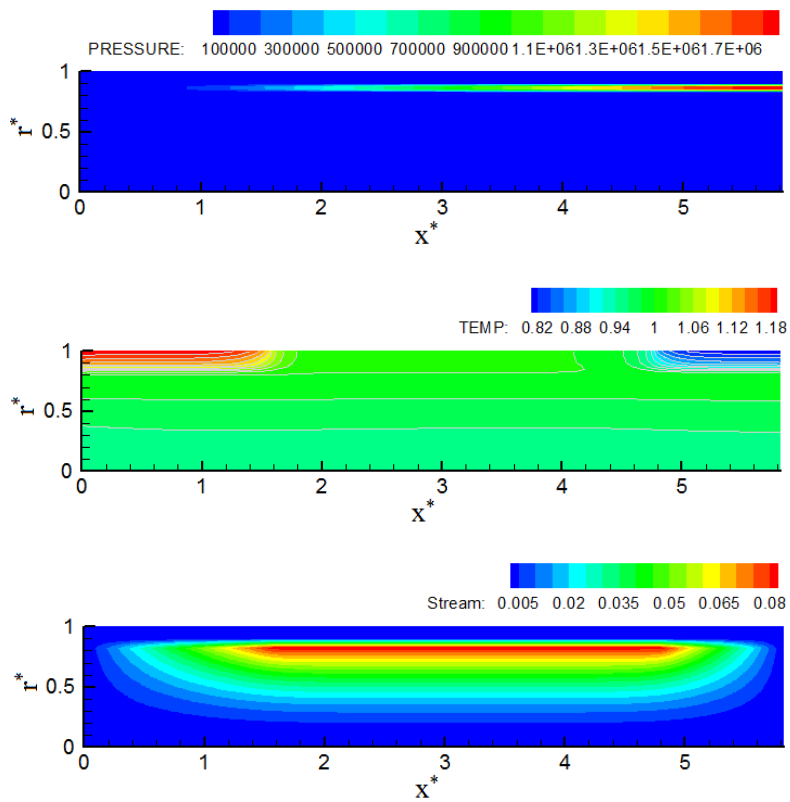


Figure 9: Dimensionless liquid pressure, temperature and Stream line distribution inside the heat pipe at $Q_{in}=5$ W and mesh number 200.

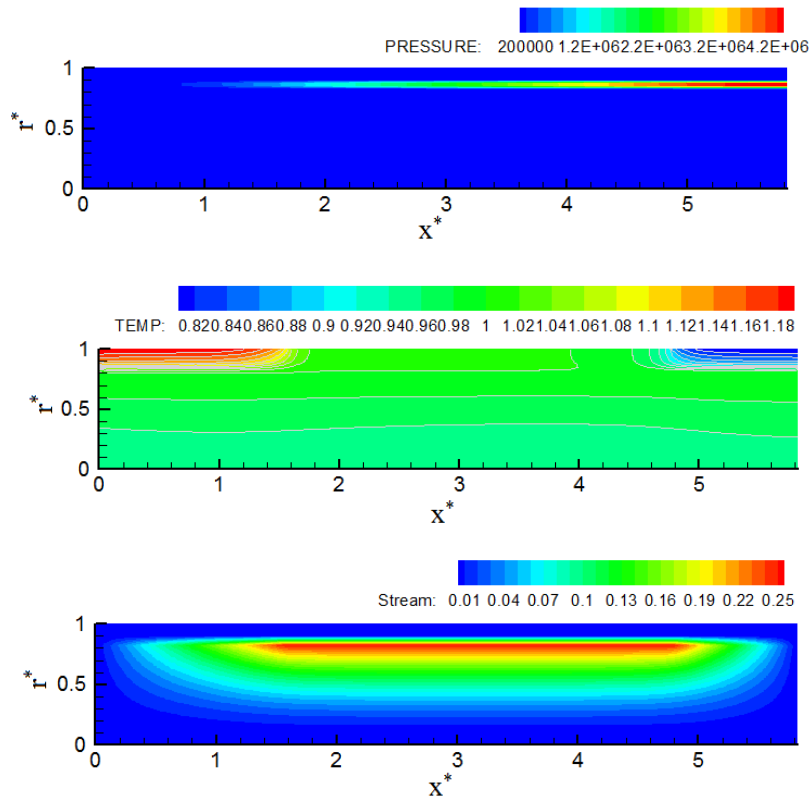


Figure 10: Dimensionless liquid pressure, temperature and Stream line distribution inside the heat pipe at $Q_{in}=15$ W and mesh number 200.

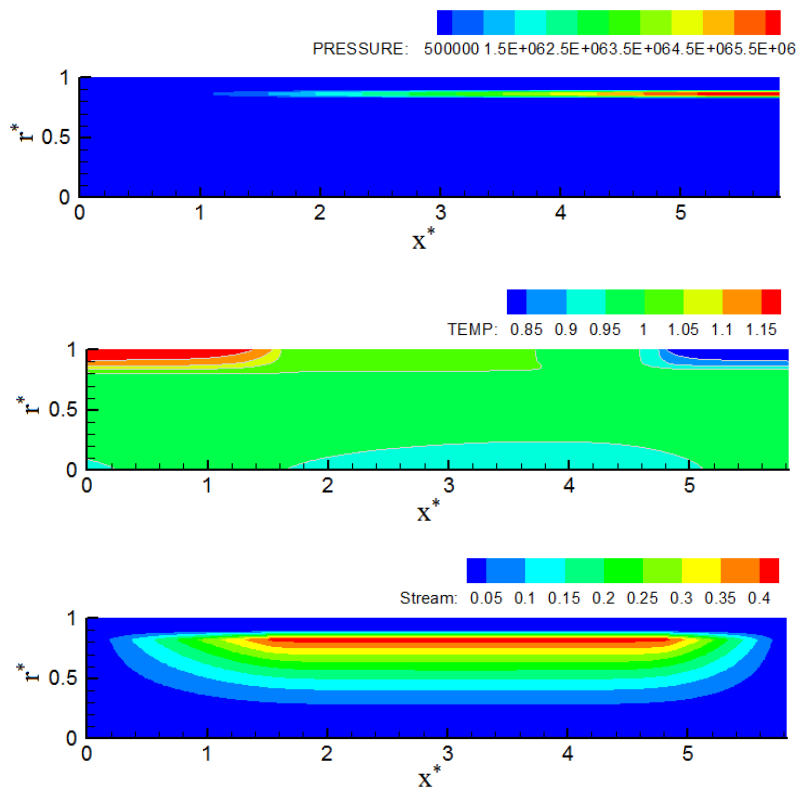


Figure 11: Dimensionless liquid pressure, temperature and Stream line distribution inside the heat pipe at $Q_{in}=25$ W and mesh number 200.

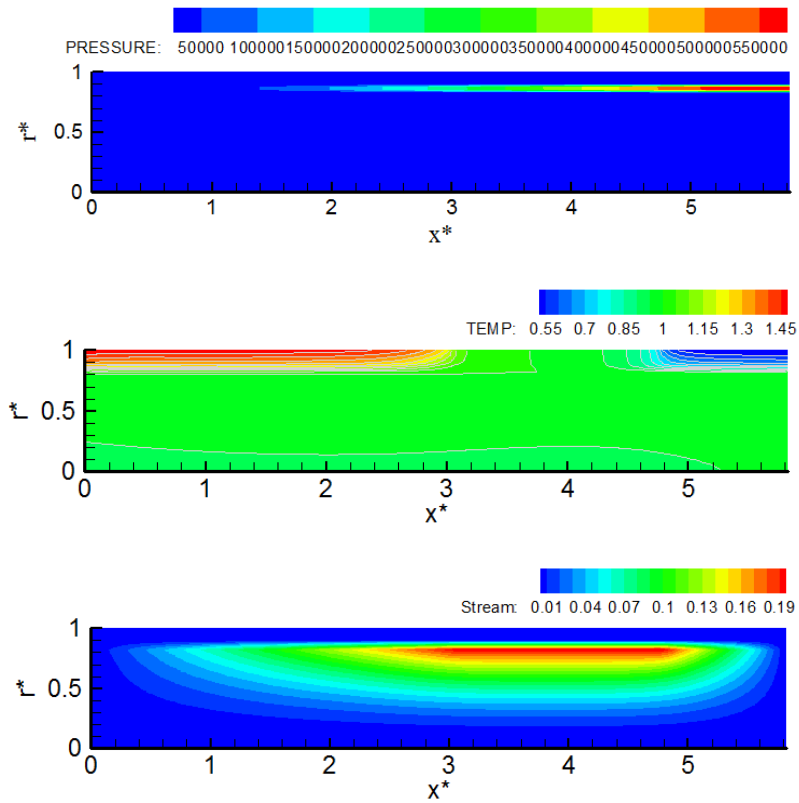


Figure 12: Dimensionless liquid pressure, temperature and Stream line distribution inside the heat pipe at $Q_{in}=15$ W, mesh number 145 and $L_e=2.99L_c$.

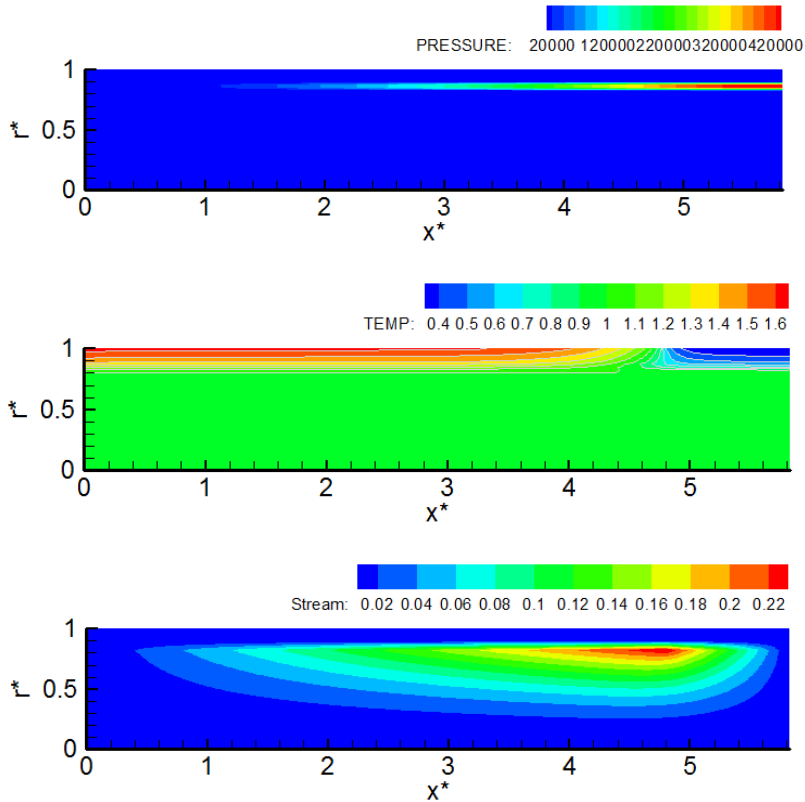


Figure 13: Dimensionless liquid pressure, temperature and Stream line distribution inside the heat pipe at $Q_{in}=15$ W, mesh number 145 and $L_e=4.721L_c$.

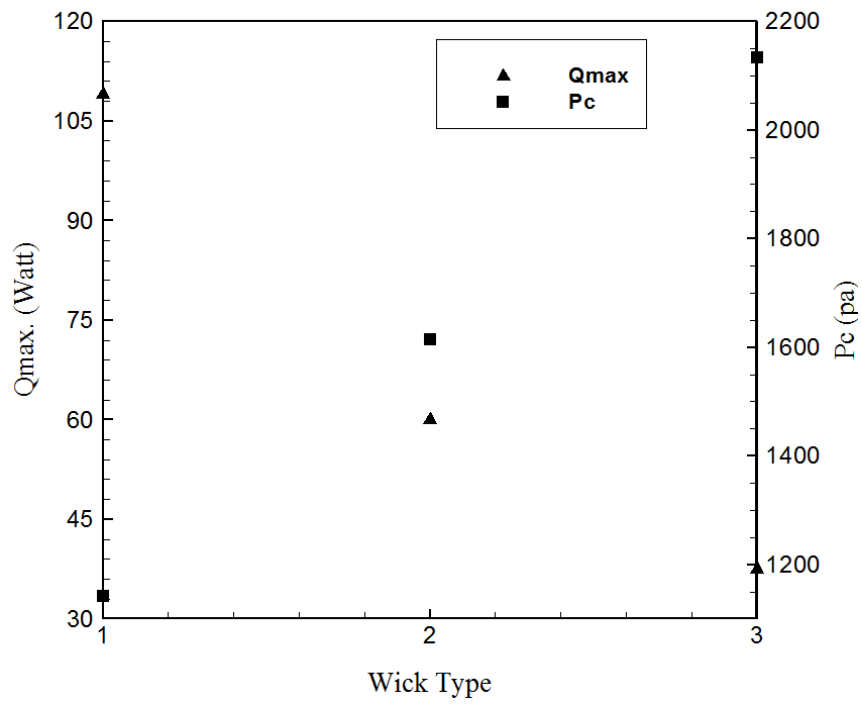


Figure 14: Maximum heat transfer limit and capillary pressure versus wick type, at $Q_{in}=25$ W.

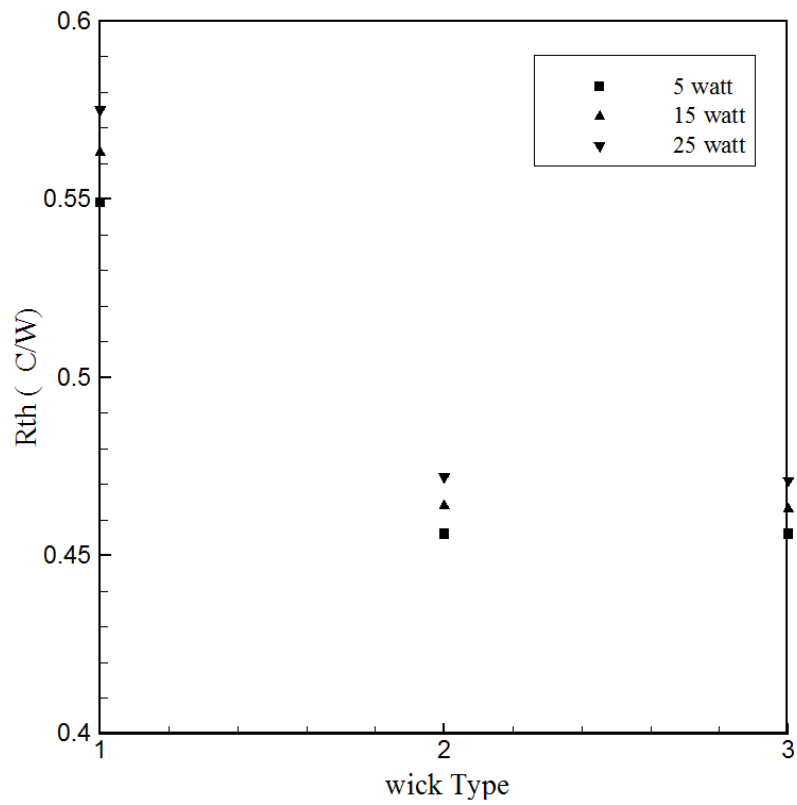


Figure 15: Heat pipe thermal resistance versus wick type.

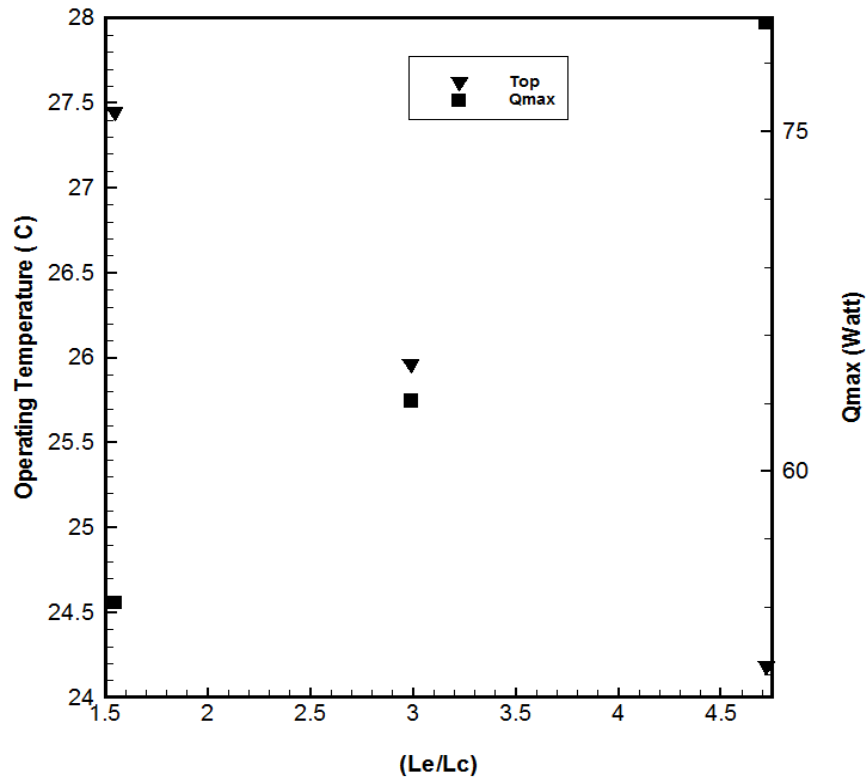


Figure 16: Heat pipe operating temperature and maximum heat transfer limit versus evaporator to condenser length ratio, at $Q_{in}=15$ W.

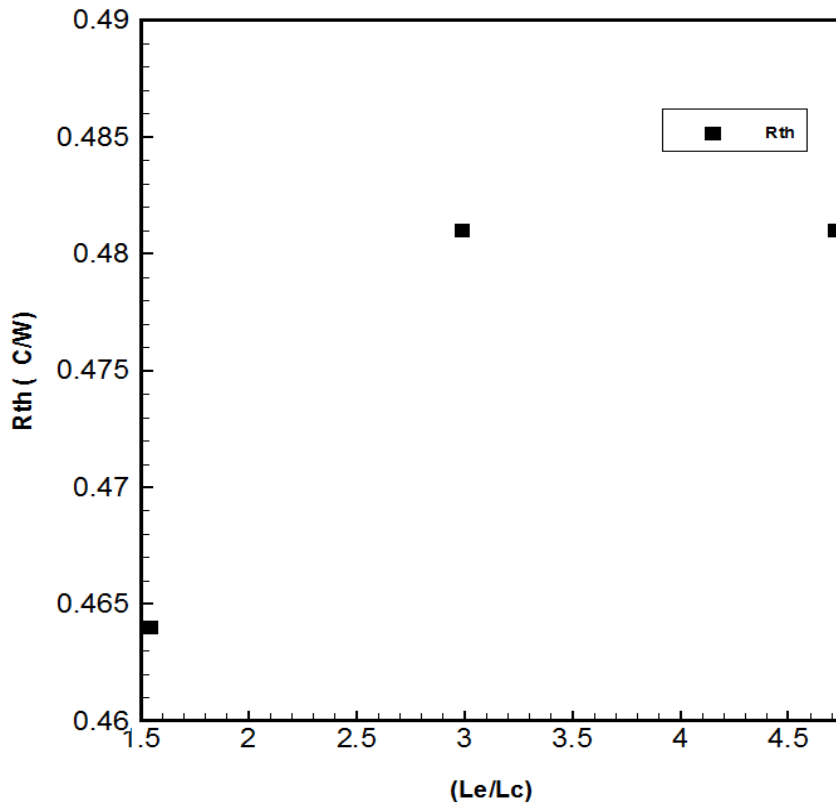


Figure 17: Heat pipe thermal resistance versus evaporator to condenser length ratio, at $Q_{in}=15$ W.

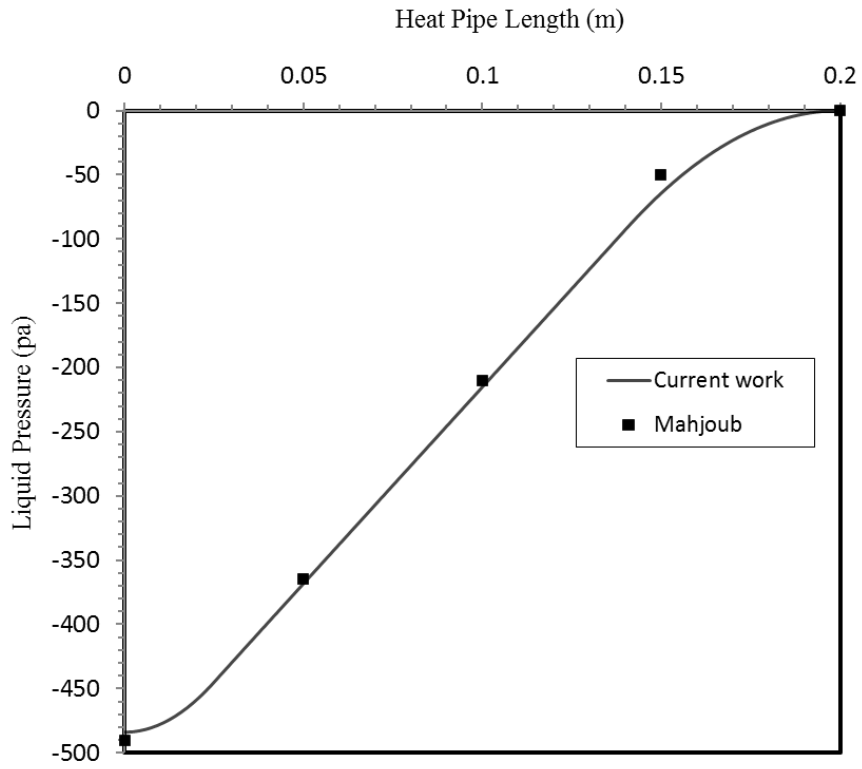


Figure 18: Comparing current model with available numerical data.